J Supercond Nov Magn (2015) 28:2855–2863
DOI 10.1007/s10948-015-3111-9

ORIGINAL PAPER

Nanoscale Clustering and Magnetic Properties of $Mn_xFe_{3-x}O_4$ Particles Prepared from Natural Magnetite

Ahmad Taufiq[1,2] · Sunaryono[1,2] · Edy Giri Rachman Putra[3] · Atsushi Okazawa[4] · Isao Watanabe[5] · Norimichi Kojima[4] · Suminar Pratapa[1] · Darminto[1]

Received: 30 April 2015 / Accepted: 11 May 2015 / Published online: 30 May 2015

Abstract A series of $Mn_xFe_{3-x}O_4$ ($0 \leq x \leq 1$) nanoparticles was successfully synthesized via a simple coprecipitation method. The starting material was a natural magnetite purified from local iron sand. Crystallite nanoparticles were produced by drying without using a high calcination temperature. Rietveld analysis of the X-ray diffractometry (XRD) data for all samples demonstrated that the Mn ions partially substituted the Fe ions in the spinel cubic structure of the Fe_3O_4 to form $Mn_xFe_{3-x}O_4$ phases. We applied two lognormal spherical and single mass fractal models to the analysis of the small-angle neutron scattering (SANS) data and revealed that the primary $Mn_xFe_{3-x}O_4$ particles ranged in size from 1.5 to 3.8 nm and formed three-dimensional clusters as secondary structures. The samples displayed superparamagnetic behavior, having the saturation magnetization which was most likely influenced by the competing contribution from Mn, the sizes of the primary particles, and their clusters. Further analysis revealed that the zero-field-cooled and field-cooled curves of the $Mn_xFe_{3-x}O_4$ nanoclusters exhibited a superparamagnetic phenomenon with the lowest magnetic blocking temperature approximately 145 K.

Keywords Nanoclusters · $Mn_xFe_{3-x}O_4$ · Coprecipitation · Saturation magnetization · Blocking temperature · Natural magnetite

1 Introduction

Magnetic nanomaterials are highly desirable due to the enormous possibilities they offer in a broad range of applications in biomedical applications [1], photothermal therapy [2], as radiosensitizers in cancer therapy [3], in hydrophobic drug delivery [4], as supercapacitors [5], in copper removal from water [6], as adsorbents of toxic heavy metals [7], and many others. Among the magnetic nanomaterials, magnetite (Fe_3O_4) nanoparticles are the most extensively studied because they can be manipulated and controlled with an external magnetic field.

Many approaches for the synthesis of magnetite nanoparticles have been developed for attaining high-quality materials with particular phase purities and particle sizes. One of the main challenges for the synthetic methods is to produce materials with a good particle size distribution and desired composition uniformity, structure and crystallinity [8]. It

✉ Darminto
darminto@physics.its.ac.id

1 Department of Physics, Faculty of Mathematics and Natural Sciences, Sepuluh Nopember Institute of Technology (ITS), Jalan Arif Rachman Hakim, Surabaya 60111, Indonesia

2 Department of Physics, Faculty of Mathematics and Natural Sciences, State University of Malang (UM), Jl. Semarang 5, Malang 65145, Indonesia

3 Center for Science and Technology of Advanced Materials, National Nuclear Agency of Indonesia (BATAN), Kawasan Puspiptek Serpong, Tangerang 15314, Indonesia

4 Department of Basic Science, Graduate School of Arts and Sciences, The University of Tokyo, Tokyo 153-8902, Japan

5 Advanced Meson Science Laboratory, Nishina Center, RIKEN, 2-1, Hirosawa, Wako, Saitama 351-0198, Japan

was recently shown that the coprecipitation approach is the simplest, most useful [9], widely used [10], most efficient, and the least expensive [11] method for the preparation of ferrous oxide nanoparticles. Additionally, it allows control over the particle size and morphology [12]. Therefore, for the abovementioned reasons, we used this method for the preparation of the nanoparticle samples.

Saturation magnetization is an important parameter for magnetite nanomaterial applications. One way to obtain a higher saturation magnetization is by introducing Mn ions to form a $Mn_xFe_{3-x}O_4$ system. Theoretically, the substitution of a Fe^{2+} ion with a Mn^{2+} ion in the system will increase its magnetization because a Mn^{2+} ion has a 25 % higher magnetic moment than a Fe^{2+} ion [13]. Several authors also reported that the particle size had a significant effect on the saturation magnetization of the $Mn_xFe_{3-x}O_4$ system [14–16]. However, they did not investigate whether there was a magnetic saturation effect originating from the clustering of the particles. To study the magnetic properties of the $Mn_xFe_{3-x}O_4$ nanoparticles in more detail, we examined their saturation magnetization dependence not only on the Mn content but also on the presence of the primary particles (or individual particles as defined by [2, 17]) and the secondary structures. The secondary structures are defined as the clusters of the primary particles. To explore these dependencies, a powerful small-angle scattering technique is required. This technique has the capability to examine the hierarchical nanostructures, the primary particles, the clusters within the samples [18], and fractal structures of the particles [19].

In this work, we report a method for $Mn_xFe_{3-x}O_4$ nanoparticle synthesis using a local magnetite powder from iron sand as the main source. We probe the particles' microstructures, particularly the primary particles, the clusters, and their associated magnetic properties. The microstructures were investigated using small-angle neutron scattering (SANS) and high-resolution transmission electron microscopy (HRTEM). The SANS data analysis was carried out using the two lognormal spherical model and the mass fractal model to reveal the size of the primary, the secondary, and the fractal structures. Finally, the saturation magnetization and the magnetic blocking temperature were investigated using a superconducting quantum interference device (SQUID) magnetometer. We also discuss the relationship between the microstructure and the corresponding magnetic properties.

2 Experimental Procedure

The synthesis of the $Mn_xFe_{3-x}O_4$ particles was conducted using a simple coprecipitation method. The starting material, magnetite powder, was extracted and purified from local iron sand using a magnetic separator. The powder was then dissolved in hydrochloric acid (HCl) and mixed with $MnCl_2\bullet\ 4H_2O$ using a magnetic stirrer followed by the drop-wise addition of ammonium hydroxide (NH_4OH) to obtain the precipitates. The HCl, $MnCl_2\bullet\ 4H_2O$, and NH_4OH were analytical grade from Sigma-Aldrich without further purification. The precipitates were washed using distilled water until a normal pH was reached. The pH, reaction time, and mixing speed were thoroughly controlled. All processes were kept at room temperature. The formation of the $Mn_xFe_{3-x}O_4$ particles was believed to occur as follows [20] with modification after the Mn doping:

$$2FeCl_3 + (1-x)FeCl_2 + xMnCl_2 \cdot 4H_2O + 8NH_4OH \rightarrow Mn_xFe_{3-x}O_4 + 8NH_4Cl + 4(1+x)H_2O \quad (1)$$

The phase characterization was carried out using X-ray diffractometry (XRD) (Philips X'pert MPD diffractometer) in the 2θ range from 20° to 70° using CuKα radiation to investigate the phase purity and the formation of the $Mn_xFe_{3-x}O_4$ particles. The size and morphology of the crystallites were investigated using HRTEM (Tecnai G^2 F20 X-Twin). A 36-m SANS spectrometer at the National Nuclear Agency of Indonesia was also employed to investigate the primary and secondary particles and fractal structures. In the SANS experiment, the scattering vector, $q = (4\pi/\lambda)\ \sin\ \theta$ ranged from 0.003 $\text{Å}^{-1} < q < 0.1\text{Å}^{-1}$, where θ and λ are the scattering angle and the neutron wavelength, respectively. Details of the instrument for the SANS experiment were provided elsewhere [21]. A data reduction program, GRASP [22], was applied to correct all the scattering data for an empty cell as the background, noise of the dark electronic current, the detector efficiency, and transmission of the samples. The scattering data were fitted using two lognormal spherical and single mass fractal models by a data analysis program, SASfit [23]. The magnetic properties of the $Mn_xFe_{3-x}O_4$ nanoparticles were investigated using a Quantum Design's MPMS SQUID magnetometer by applying magnetic sweeping from 5 to −5 T. The zero-fieldcooled (ZFC) and fieldcooled (FC) protocols were carried out to examine the magnetic blocking temperature of the $Mn_xFe_{3-x}O_4$ particles according to the literature [24]. The ZFC patterns were attained by cooling the samples (without applying an external magnetic field) from 400 to 5 K, and then the magnetization data (at an external magnetic field of 5 Oe) was collected during the heating process from 5 to 400 K. Furthermore, the FC patterns were obtained during the cooling process over the same temperature range and in the same field. Finally, the magnetic properties of the $Mn_xFe_{3-x}O_4$ particles were correlated with their nanostructures obtained from the SANS data analysis.

3 Results and Discussion

XRD patterns of all the samples are displayed in Fig. 1. The data confirm the presence of only magnetite (PDF No. 19-0629) without any impurities for all samples. The broad peaks had an average full-width at half-maximum (FWHM) of $> 2^\circ$ 2θ, suggesting that the magnetite exhibits a nanometric dimension [25]. Moreover, the diffraction peaks shift to a lower angle as x increases, implying that the lattice parameter increases with Mn^{2+} incorporation. The increasing lattice parameter and the crystal volume of the magnetite system are shown in Fig. 2. The increase can be attributed to the fact that the ionic radius of Mn^{2+} (0.89 Å) is larger than that of Fe^{2+} (0.77 Å) and Fe^{3+} (0.64 Å) [26]. This provides evidence that Mn^{2+} ions were successfully inserted into Fe_3O_4 [27] by partially replacing Fe^{2+} or Fe^{3+} ions to form $Mn_xFe_{3-x}O_4$. Additionally, the lattice parameters of the $Mn_xFe_{3-x}O_4$ nanoparticles increased from 8.377 to 8.439 Å. This indication of successful incorporation has also been reported by others for powder [28], film [29], and single crystal microspheres [26].

In our previous work, the XRD data analysis of the Fe_3O_4 prepared by the coprecipitation method followed by the calcination at a higher temperature showed that the nanoparticles had a crystal size of approximately 16 nm [25]. However, due to the limitation of XRD for studying the hierarchical size of nanostructures, we have not yet been able to explain in detail the particle size and clustering. In this work, the details of the particle size, particularly the primary and secondary structures, i.e., their nanosized clustering, is investigated using SANS and HRTEM.

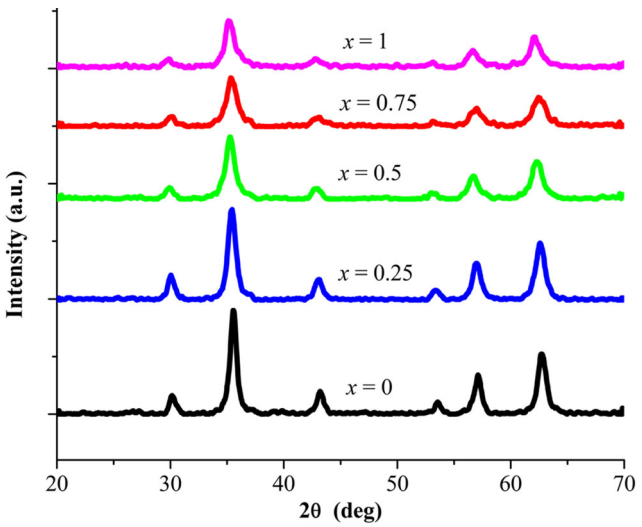

Fig. 1 XRD patterns (using CuKα radiation) of the $Mn_xFe_{3-x}O_4$ ($0 \leq x \leq 1$) powders prepared by the coprecipitation method

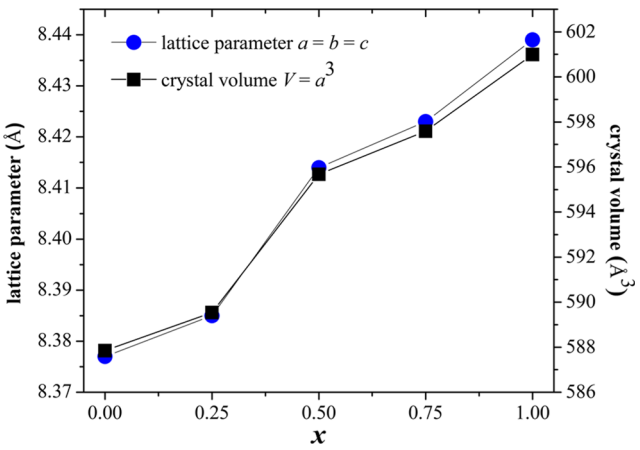

Fig. 2 Lattice parameter and crystal volume of the $Mn_xFe_{3-x}O_4$ ($0 \leq x \leq 1$) powders after the Rietveld analysis of the XRD data, as shown in Fig. 1

The composition and cationic distributions of the $Mn_xFe_{3-x}O_4$ particles for x composition between 0 and 1 can be analyzed using the following formula [30]:

$$\left(Mn_x^{2+}Fe_{1-x}^{3+}\right)\left[Fe_{1-x}^{2+}Fe_{1+x}^{3+}\right] \quad (2)$$

The iron metal ions (Fe^{2+} and Fe^{3+}) enclosed in the square bracket represent those in the octahedral positions, while the other metal ions (Mn^{2+} and Fe^{3+}) in the round bracket represent those in the tetrahedral positions depending on the x value. Six oxygen atoms surround the metal ions in the octahedral sites, while four oxygen atoms surround the metal ions in the tetrahedral sites. In the $Mn_xFe_{3-x}O_4$ system, the spinel structure can be classified into three types: inverse, mixed, and normal spinel. The structure for $x = 0$ is inverse spinel, which has eight Fe^{3+} ions located in the tetrahedral sites and eight Fe^{2+} and eight Fe^{3+} ions randomly placed in the octahedral sites [31]. The systems for $x = 0.25$, 0.5, and 0.75 form mixed spinel structure because Mn^{2+} ions partially shift the Fe^{3+} ions in the tetrahedral positions. Furthermore, the structure for $x = 1$ constructs normal spinel in which the tetrahedral sites are fully occupied by Mn^{2+} ions and the other site is fully occupied by Fe^{3+} ions.

The SANS curves of the $Mn_xFe_{3-x}O_4$ nanoparticles for x composition, $0 \leq x \leq 1$, are presented in Fig. 3. The SANS curve at a high q range represent the behavior of primary (small) particles in the samples. Meanwhile, the curves at medium and low $q$ranges explain the secondary particles and fractal dimension, respectively. Visually, the curves at the high q range for $x = 0$ and 0.25 exhibit similar trends corresponding to similar primary particle sizes, while for $x = 0.5$, 0.75, and 1, different trends occur that correspond to smaller primary particle sizes. The curves at a medium q represent the different trends associated with the differences in the secondary particles, and the curves at

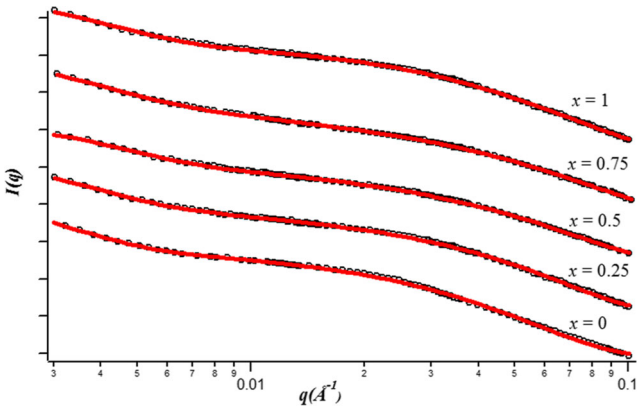

Fig. 3 SANS curves and fitting model of the $Mn_xFe_{3-x}O_4$ ($0 \le x \le 1$) nanoparticles. The data were shifted for clarity. The *circles* represent the SANS data, and the *solid lines* represent the fitting model using the two lognormal spherical model and the single mass fractal model

the low q range show a relatively similar gradient that corresponds to the similar fractal dimension of the samples. However, this qualitative analysis cannot be used to justify the detail and exact microstructures of the systems. To further examine the primary and secondary particles and the fractal dimensions simultaneously, the SANS data analysis using mathematical models with a global fitting approach is required.

All the SANS curves were fitted by assuming a two lognormal spherical model for the size distributions of the primary and secondary structures as form factor and a single structure factor for the mass fractal model [32] according to

$$I(q) \approx \int_0^\infty N_1(R_1)F_N^2(q, R_1)dR_1S(q, \xi, D, R_1) + \int_0^\infty N_2(R_2)F_N^2(q, R_2)dR_2S(q, \xi, D, R_2) \quad (3)$$

where $N$is the number density of the particles, $F(q, R)$ is the scattering amplitude, and$S(q, \xi, D, R)$ is the structure factor for a mass fractal. The curves were fitted and satisfied by two lognormal spherical models and a single structure factor model using mass fractal for the clusters. Equation (3) can then be rewritten as follows:

$$I(q) \approx \int_0^\infty N_1(R_1)F_N^2(q, R_1)dR_1 + \int_0^\infty N_2(R_2)F_N^2(q, R_2)dR_2S(q, \xi, D, R_2) \quad (4)$$

For the particle size distribution of the magnetic nanoparticles, the lognormal function is the best model to describe the size distribution of the particle radii [33]. For spherical particles with a diameter, $D = 2R$, it is modified from [34]

$$N(R) = P(R) = \frac{1}{\sigma R\sqrt{2\pi}} \exp\left(-\frac{(\ln R - \ln R_0)^2}{2\sigma^2}\right) \quad (5)$$

where R_0 and σ are the characteristic radius of the distribution and standard deviation or polydispersity index, respectively. The structure factor S for a mass fractal [35] is given as

$$S(q) = 1 + \frac{D\Gamma(D-1)}{(qR)^D\left[1 + 1/(q^2\xi)^2\right]^{(D-1)/2}} \times \sin\left[(D-1)\tan^{-1}(q\xi)\right] \quad (6)$$

where $q$is the scattering vector, Γ is a gamma function, D is the fractal dimension, and ξ is the cutoff distance. The results of the pattern analysis of the SANS curves of the $Mn_xFe_{3-x}O_4$ nanoparticles are displayed in Table 1.

According to Table 1, when the Mn content becomes larger, the size of the $Mn_xFe_{3-x}O_4$ ($0 \le x \le 1$) nanoparticles becomes smaller. In general, small particles (with radius R_1) as primary particles construct larger particles or secondary structures (with radius R_2) as clusters with agglomeration and/or aggregation [17]. The cluster formation is affected by the magnetic interparticle interactions between the nanoparticles [18] and the fractal dimension, indicating that a reaction-limited mechanism occurs in the magnetic nanoparticles system [36]. The fractal dimension of $Mn_xFe_{3-x}O_4$ tends to be similar to 3, corresponding to the growth of the structures in three dimensions. Such a

Table 1 Result of the fits for the SANS data using Fig. 3. and Eqs. 3–6 for the $Mn_xFe_{3-x}O_4$ nanoparticles

Sample x	R_1 (nm)	R_2 (nm)	D
0	3.8	9.3	2.9
0.25	3.8	9.6	2.7
0.5	2.2	7.8	2.5
0.75	1.9	5.7	2.7
1	1.5	5.2	2.8

*D*value can be associated with a construction of a three-dimensional building block. To achieve a stable state, the magnetic nanoparticles with a high surface free energy tend to cluster. Therefore, the formation of clusters leads to the reduction of the surface area of the magnetic nanoparticles [37]. Additionally, the magnetic nanoparticles with smaller particle sizes have a larger affinity to aggregate into clusters, which is related to the lower energy barriers [38].

Further insight into the morphology and structure of the samples, which is represented by $x = 0.5$, is provided by the HRTEM images shown in Fig. 4. The primary particles have a radius of approximately 2.5 nm, and the secondary structures form clusters that have a radius of approximately 8 nm when compared with the results from the SANS data. These results are in a good agreement with the work by Giri and coworkers in which the TEM photographs of their $Mn_{0.4}Fe_{2.6}O_4$ nanoparticles showed nearly a spherical shape with a radius of approximately 12 nm and nanoclusters [39]. In addition, Fig. 4 also shows that the $Mn_{0.5}Fe_{2.5}O_4$ sample has a high crystalline nature with the lattice parameter scale approximately 0.8 nm, which corresponds to the XRD data presented in the above discussion.

Figure 5 shows the magnetic hysteresis loop of the $Mn_xFe_{3-x}O_4$ nanoparticles via the SQUID magnetometer with the applied magnetic field sweeping from −5 to 5 T at room temperature. The figure shows that the samples exhibit the patterns with nearly negligible coercive forces and remanent magnetizations. Therefore, the prepared $Mn_xFe_{3-x}O_4$ nanoparticles exhibit superparamagnetic properties. In good agreement with this work, another experiment showed that the magnetic nanoparticles exhibit remanent magnetization and a coercive force that is approximately negligible, indicating superparamagnetic behavior [40]. The phenomenon of superparamagnetism can be explained by the size effects and thermal fluctuations. The superparamagnetic behavior occurs when the particle sizes are smaller than the critical size, and the thermal fluctuations lead to spontaneous demagnetization of the preceding saturated assembly of the magnetic nanoparticles [41]. The samples have a random orientation in the absence of an external magnetic field; however, under the presence of one, the moment orientates parallel to the field direction and achieves its saturation [42].

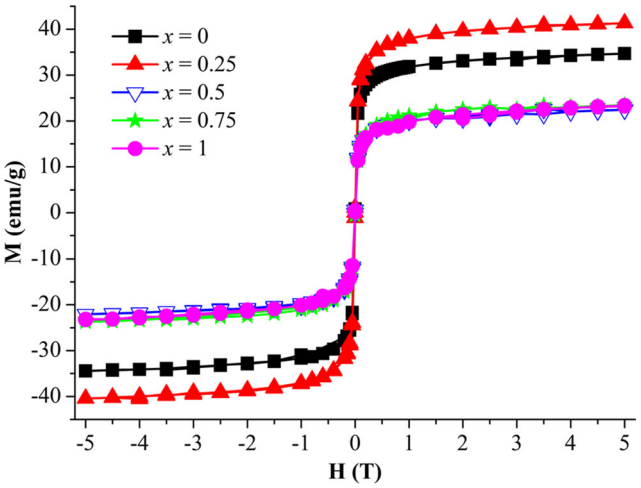

Fig. 5 Magnetic hysteresis loops of the $Mn_xFe_{3-x}O_4$ nanoparticles at 300 K

More detailed studies on the superparamagnetic properties of the $Mn_xFe_{3-x}O_4$ nanoparticles can be conducted using a ZFC-FC measurement, as displayed in Fig. 6. As shown, the maximum peak of the ZFC curve tends to shift to lower temperature as x increases. The maximum peak observed in the ZFC curve is defined as the magnetic blocking temperature (T_B) [43–45] and occurs where the anisotropy energy barrier is comparable to the thermal energy of the particles. Due to the effect of magnetic randomization, the magnetic nanoparticles do not magnetically interact above T_B; however, they do interact and exhibit ferromagnetic-like properties below T_B [46]. In general, starting from the low temperature region, the magnetization in the ZFC curve increases until a maximum is achieved at T_B and then decreases. The FC curve is nearly stable below

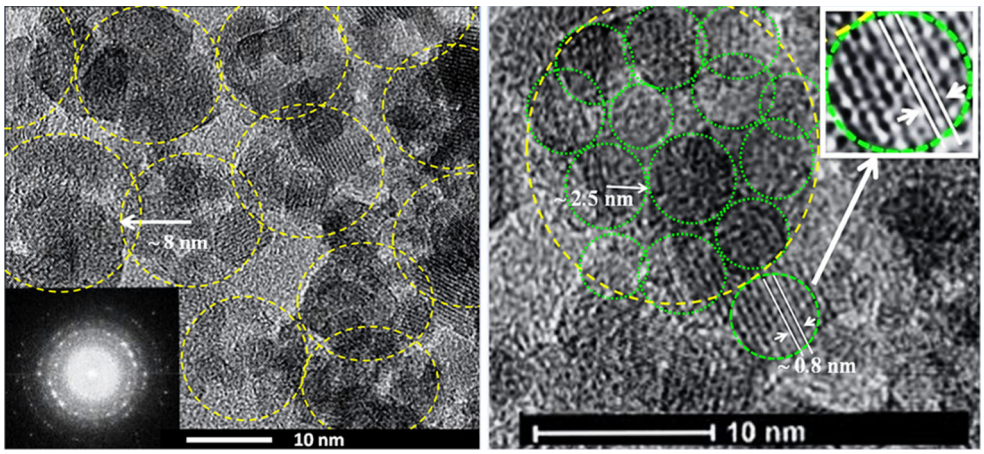

Fig. 4 HRTEM image of $Mn_{0.5}Fe_{2.5}O_4$ sample. The *green circles* represent the primary particles, and the *yellow circles* represent the secondary particles

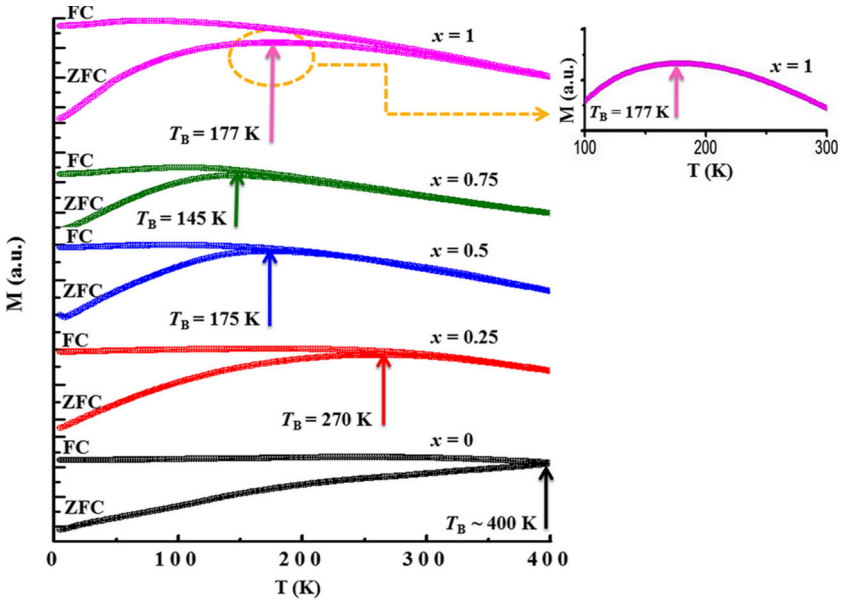

Fig. 6 Magnetization (ZFC-FC curves) of the $Mn_xFe_{3-x}O_4$ nanoparticles as a function of temperature. For clarity, the curves were shifted, and the ZFC curve for $x = 1$ was zoomed out (*upper right picture*) around its T_B

T_B, and it overlaps with the ZFC curve above T_B. The temperature at which the magnetization data in the ZFC and FC curves starts to bifurcate is defined as the transition [47] or magnetic irreversibility [48, 49] temperature. Here, the transition and blocking temperatures in the ZFC and FC curves are similar, except for $x = 1$. The separating magnetizations of the ZFC and FC curves of the magnetic nanoparticles correspond to the de-blocking of their magnetic moments [50]. In ideal monodisperse magnetic nanoparticles, the blocking and transition temperatures should overlap at the same point [39]. However, due to the van der Waals or molecular forces in magnetic nanoparticles, it is difficult to obtain monodispersed nanoparticle samples.

In this experiment, the T_B values of the $Mn_xFe_{3-x}O_4$ nanoparticles decrease with x, which is in good agreement with other experimental results [39]. According to Table 1, higher x values correspond to smaller sized primary particles and clusters, which significantly relates to the reduced T_B. T_B, which indicates the transition between the blocked state and superparamagnetic behavior is strongly dependent on the particles size of the nanoparticles as displayed in the following equation [51]:

$$T_B = \frac{KV}{25k_B} \tag{7}$$

where k_B and K are Boltzmann's constant and the anisotropy constant, respectively, and V represents the particle size (volume).

Dutta and coworkers reported that the T_B decreased upon reducing the particle size of the magnetic nanoparticles [52]. Meanwhile, Rumpf et al. reported that the T_B was also dependent on the particle-particle distance [46], and their samples exhibited superparamagnetism and followed the Curie-Weiss law above the T_B in which the thermal energy was larger than the magnetic energy barrier [47]. Therefore, we presume that the $Mn_xFe_{3-x}O_4$ nanoparticles exhibited superparamagnetic behavior at room temperature, except for $x = 0$ in which the T_B is higher than room temperature. To better understand the magnetic properties of these superparamagnetic materials, the saturation magnetization of the $Mn_xFe_{3-x}O_4$ nanoparticles is discussed as follows.

To understand the saturation magnetizations (M_s) due to the effect of the Mn contents, we tabulated the data in Table 2. Based on Fig. 5 and Table 2, the saturation magnetization of the $Mn_xFe_{3-x}O_4$ nanoparticles increases from $x = 0$ to $x = 0.25$, but it decreases and remains stable for $x = 0.5$, 0.75, and 1. However, based on the theoretical prediction, substituting Fe^{2+} by Mn^{2+} ions in the system of the $Mn_xFe_{3-x}O_4$ nanoparticles increases their

Table 2 Saturation magnetization of the $Mn_xFe_{3-x}O_4$ nanoparticles, calculated from Fig. 5

Sample x	M_s (emu/g)	Delta M_s (%)
0	34.69	0.0
0.25	41.31	19.1
0.5	22.44	−35.3
0.75	23.47	−32.3
1	23.38	−32.6

magnetization because Mn^{2+} (5 μ B) has a higher magnetic moment than Fe^{2+} (4 μ B) [13]. The different magnetic moments of Mn^{2+}, Fe^{2+}, and Fe^{3+} located between the tetrahedral and octahedral sites have contributed to the saturation magnetization of $Mn_xFe_{3-x}O_4$. The interaction of the antiparallel spin-coupling occurring between Fe and Mn ions in the tetrahedral and octahedral sites corresponds to antiferromagnetism. However, the incomplete cancellation of the spin moments contributes to the net ferromagnetic moments; thus, the saturation magnetization of the $Mn_xFe_{3-x}O_4$ system can be calculated using the net magnetic moment. The $Mn_xFe_{3-x}O_4$ system exhibits a linear increase in magnetic moment of $4 + x$ μ_B in the Bohr magneton per formula unit [39]. For $x = 0.25$, the saturation magnetization increases by approximately 19.1 % from $x = 0$, which is higher than the theoretical calculation that was predicted to be approximately 6.25 %. In this case, the primary particles of $x = 0$ and $x = 0.25$ are similar, but their clusters are different. Therefore, this increases the saturation magnetization (12.85 %) due to the effect of the increasing Mn doping and particle sizes of the clusters. Recently, Shen et al. reported that the magnetite nanoparticles in bigger clusters have a higher saturation magnetization than smaller clusters and individual particles [2], which is in accordance with this experiment. Further, for $x = 0.5$, 0.75, and 1, the theoretical calculation of the saturation magnetization increased by approximately 12.5, 18.75, and 25 %, respectively. However, in this experiment, they have smaller values than those of $x = 0$ and 0.25. This reduced value is predicted to be an effect of the reduced size of the primary particles and clusters. In accordance with this result, another experimental report also showed that the saturation magnetization of the magnetic nanoparticles was affected by the size of their primary particles and clusters [53]. In addition, Goya et al. reported that the saturation magnetization decreases for smaller particles, which is associated with the increasing effects of the spin disorder at the surface of the particles, yielding a reduction in the net magnetic moment [54].

Wang and coworkers reported that the saturation magnetizations of $Mn_xFe_{3-x}O_4$ films are different from the theoretical prediction, so they recommended a modified growth process [29]. In single crystalline microspheres, the saturation magnetization decreased significantly from $x = 0$ to $x = 1$ due to the weaker spin-spin interaction [26]. Meanwhile, in the $Zn_xFe_{3-x}O_4$ system, the saturation magnetizations exhibited an arbitrary trend for $x < 0.3$ and reduced for $x \geq 0.3$, which was strongly affected by the Zn^{2+} contents and their particle sizes [55]. The magnetic properties of nanoparticles are also influenced by dead layer formation on the surface, random canting of particle surface spins, particle random distribution in the resulting non-saturation effect, cation site disorder, and the presence of adsorbed water [10]. Therefore, despite the Mn doping effect, other mechanisms could explain the saturation magnetizations of $Mn_xFe_{3-x}O_4$ nanoparticles. Furthermore, to study the magnetic saturation of $Mn_xFe_{3-x}O_4$ as the only effect on the Mn contents, certain parameters should be controlled by controlling the parameters during synthesis. However, this is still a challenge that needs to be solved for the synthesis of $Mn_xFe_{3-x}O_4$ in several forms, such as in micro- or nanosized particles with special shapes, single crystalline microspheres, thin or thick films, and fluid systems. Based on our SANS experiments, we conclude that the Mn contents and particle sizes, such as the primary particles and their clustering, are the most probable combined effects that play a role in saturated magnetizations.

4 Conclusions

Single-phase $Mn_xFe_{3-x}O_4$ ($0 \leq x \leq 1$) nanoclusters have been successfully prepared from natural magnetite using a simple coprecipitation method. The Mn ions successfully substituted the Fe ions into the Fe_3O_4 nanoparticles and increased their lattice parameters. The data analysis of the SANS profiles revealed that all samples had primary particles ranging from 1.5 to 3.8 nm, and they tended to construct clusters in three-dimensional structures. The M-H curves showed that all samples exhibited superparamagnetic behavior. The saturation magnetizations of the $Mn_xFe_{3-x}O_4$ nanoparticles increased from $x = 0$ to $x = 0.25$, but they decreased and remained stable for $x = 0.5$, 0.75, and 1. This phenomenon was caused by the Mn content, the size of the primary particles, and the clusters of the $Mn_xFe_{3-x}O_4$ nanoparticles. Furthermore, the magnetic blocking temperature of the samples, which was acquired from the ZFC-FC curves, is strongly correlated with the size of the particles, and the lowest value was 145 K.

Acknowledgments The authors would like to thank Dr. Mauro Porcu for the HRTEM characterization and the University of Tokyo, the RIKEN Nishina Center Japan, and the Neutron Scattering Laboratory at BATAN Serpong for the use of their characterization facilities. This research was partially supported by the BPPS and PKPI Programs from the Ministry of Education and Culture, Republic of Indonesia (A.T. and S.), "Penelitian Disertasi Doktor" (A.T.), and also "Hibah Kompetensi" of DP2M, Ditjen DIKTI, 2013-2015 (D.).

References

1. Shete, P.B., Patil, R.M., Tiwale, B.M., Pawar, S.H.: Water dispersible oleic acid-coated Fe_3O_4 nanoparticles for biomedical applications. J. Magn. Magn. Mater. **377**, 406–410 (2015)

2. Shen, S., Wang, S., Zheng, R., Zhu, X., Jiang, X., Fu, D., Yang, W.: Magnetic nanoparticle clusters for photothermal therapy with near-infrared irradiation. Biomaterials **39**, 67–74 (2015)
3. Meidanchi, A., Akhavan, O., Khoei, S., Shokri, A.A., Hajikarimi, Z., Khansari, N.: $ZnFe_2O_4$ nanoparticles as radiosensitizers in radiotherapy of human prostate cancer cells. Mater. Sci. Eng. C **46**, 394–399 (2015)
4. Ding, Y., Shen, S.Z., Sun, H., Sun, K., Liu, F., Qi, Y., Yan, J.: Design and construction of polymerized-chitosan coated Fe_3O_4 magnetic nanoparticles and its application for hydrophobic drug delivery. Mater. Sci. Eng. C **48**, 487–498 (2015)
5. Raj, B.G.S., Ramprasad, R.N.R., Asiri, A.M., Wu, J.J., Anandan, S.: Ultrasound assisted synthesis of Mn_3O_4 nanoparticles anchored graphene nanosheets for supercapacitor applications. Electrochimica Acta **156**, 127–137 (2015)
6. Ghaemi, N., Madaeni, S.S., Daraei, P., Rajabi, H., Zinadini, S., Alizadeh, A., Heydari, R., Beygzadeh, M., Ghouzivand, S.: Polyethersulfone membrane enhanced with iron oxide nanoparticles for copper removal from water: application of new functionalized Fe_3O_4 nanoparticles. Chem. Eng. J **263**, 101–112 (2015)
7. Ahalya, K., Suriyanarayanan, N., Ranjithkumar, V., et al.: Effect of cobalt substitution on structural and magnetic properties and chromium adsorption of manganese ferrite nano particles. J. Magn. Magn. Mater. **372**, 208–213 (2014)
8. Martínez-Mera, I., Espinosa-Pesqueira, M.E., Pérez-Hernández, R., Arenas-Alatorre, J.: Synthesis of magnetite (Fe_3O_4) nanoparticles without surfactants at room temperature. Mater. Lett **61**, 4447–4451 (2007)
9. Amirabadizadeh, A., Farsi, H., Dehghani, M., Arabi, H.: Effect of substitutions of Zn for Mn on size and magnetic properties of Mn–Zn ferrite nanoparticles. J. Supercond. Nov. Magn. **25**, 2763–2765 (2012)
10. Sharifi, I., Shokrollahi, H., Amiri, S.: Ferrite-based magnetic nanofluids used in hyperthermia applications. J. Magn. Magn. Mater. **324**, 903–915 (2012)
11. Niu, J.M., Mei, J.: Effect of temperature on Fe_3O_4 magnetic nanoparticles prepared by coprecipitation method. Adv. Mater. Res. **900**, 172–176 (2014)
12. Darminto, Cholishoh, M.N., Perdana, F.A., Baqiya, M.A., Mashuri, Cahyono, Y., Triwikantoro: Preparing Fe_3O_4 nanoparticles from Fe^{2+} ions source by co-precipitation process in various pH. AIP Conference Proceedings, pp. 234–237. AIP Publishing (2011)
13. Cullity, B.D., Graham, C.D.: Introduction to magnetic materials. Wiley-IEEE Press, Hoboken (2008)
14. Upadhyay, R., Davies, K., Wells, S., Charles, S.: Preparation and characterization of ultra-fine $MnFe_2O_4$ and $Mn_xFe_{1-x}Fe_2O_4$ spinel systems: I particles. J. Magn. Magn. Mater. **132**, 249–257 (1994)
15. Saravanan, P., Alam, S., Kandpal, L.D., Mathur, G.N.: Effect of substitution of Mn ion on magnetic properties of Fe_3O_4 nanocrystallites. J. Mater. Sci. Lett. **21**, 1135–1137 (2002)
16. Doaga, A., Cojocariu, A.M., Amin, W., Heib, F., Bender, P., Hempelmann, R., Caltun, O.F.: Synthesis and characterizations of manganese ferrites for hyperthermia applications. Mater. Chem. Phys. **143**, 305–310 (2013)
17. Kim, B., Yang, J., Lim, E.-K., Park, J., Suh, J.-S., Park, H., Huh, Y.-M., Haam, S.: Double-ligand modulation for engineering magnetic nanoclusters. Nanoscale Res. Lett. **8**, 104 (2013)
18. Shtykova, E.V., Huang, X., Remmes, N., Baxter, D., Stein, B., Dragnea, B., Svergun, D.I., Bronstein, L.M.: Structure and properties of iron oxide nanoparticles encapsulated by phospholipids with poly(ethylene glycol) tails. J. Phys. Chem. C **111**, 18078–18086 (2007)
19. Sari, W., Fitriyani, D., Putra, E.G.R., bin Mohamed, A.A., Ibrahim, N.: Fractal structures on silica aerogels containing titanium: a small angle neutron scattering study. AIP Conf. Proc. **1202**, 185–188 (2010)
20. Bajpai, A.K., Likhitkar, S.: Investigation of magnetically enhanced swelling behaviour of superparamagnetic starch nanoparticles. Bull. Mater. Sci. **36**, 15–24 (2013)
21. Putra, E.G.R., Bharoto, Santoso, E., Ikram, A.: Improved performances of 36 m small-angle neutron scattering spectrometer BATAN in Serpong Indonesia. Nucl. Instrum. Methods Phys. Res. Sect. Accel. Spectrometers Detect. Assoc. Equip. **600**, 198–202 (2009)
22. Dewhurst, C.: GRASANSP: graphical reduction and analysis SANS program for Matlab (2001)
23. Kohlbrecher, J., Bressler, I.: Software package SASfit for fitting small-angle scattering curves (2011)
24. Suzuki, M., Fullem, S.I., Suzuki, I.S., Wang, L., Zhong, C.-J.: Observation of superspin-glass behavior in Fe_3O_4 nanoparticles. Phys. Rev. B **79**, 024418 (2009)
25. Pratapa, S., Susanti, L., Insany, Y.A.S., Alfiati, Z., Hartono, B., Mashuri, Taufiq, A., Fuad, A., Triwikantoro, Baqiya, M.A., Purwaningsih, S., Yahya, E.: Darminto: XRD line-broadening characteristics of M-oxides (M = Mg, Mg-Al, Y, Fe) nanoparticles produced by coprecipitation method. AIP Conf. Proc. **1284**, 125–128 (2010)
26. Li, Y.H., Kouh, T., Shim, I.-B., Kim, C.S.: Investigation of cation distribution in single crystalline $Fe_{3-x}Mn_xO_4$ microspheres based on Mössbauer spectroscopy. J. Appl. Phys. **111**, 07B544 (2012)
27. Yoon, H., Lee, J., Min, J., Wu, J., Kim, Y.: Synthesis, microstructure, and magnetic properties of monosized $Mn_xZn_yFe_{3-x-y}O_4$ ferrite nanocrystals. Nanoscale Res. Lett. **8**, 530 (2013)
28. Amighian, J., Karimzadeh, E., Mozaffari, M., et al.: The effect of Mn^{2+} substitution on magnetic properties of $Mn_xFe_{3-x}O_4$ nanoparticles prepared by coprecipitation method. J. Magn. Magn. Mater. **332**, 157–162 (2013)
29. Wang, K.M., Lee, D.S., Horng, L., Chern, G.: Structural and magnetic properties of $Fe_{3-x}Mn_xO_4$ films. Int. Symp. Adv. Magn. Technol. **282**, 73–77 (2004)
30. Wickham, D.G.: The chemical composition of spinels in the system Fe_3O_4-Mn_3O_4. J. Inorg. Nucl. Chem. **31**, 313–320 (1969)
31. Mazo-Zuluaga, J., Restrepo, J., Mejía-López, J.: Effect of surface anisotropy on the magnetic properties of magnetite nanoparticles: a Heisenberg–Monte Carlo study. J. Appl. Phys. **103**, 113906_1–113906_8 (2008)
32. Yusuf, S.M., Mukadam, M.D., De Teresa, J.M., Ibarra, M.R., Kohlbrecher, J., Heinemann, A., Wiedenmann, A.: Structural and magnetic properties of amorphous iron oxide. Phys. B Condens. Matter. **405**, 1202–1206 (2010)
33. Paula, F.L.O., Aquino, R., da Silva, G.J., Depeyrot, J., Tourinho, F.A., Fossum, J.O., Knudsen, K.D.: Small-angle X-ray and small-angle neutron scattering investigations of colloidal dispersions of magnetic nanoparticles and clay nanoplatelets. J. Appl. Crystallogr., s269–s273 (2007)
34. Gadhvi, M., Upadhyay, R.V., Parekh, K., Mehta, R.V.: Magnetically textured ferrofluid in a non-magnetic matrix: magnetic properties. Bull. Mater. Sci. **27**, 163–168 (2004)
35. Teixeira, J.: Small-angle scattering by fractal systems. J. Appl. Crystallogr. **21**, 781–785 (1988)
36. Putra, E.G.R., Seong, B.S., Shin, E., Ikram, A., Ani, S.A., Darminto: Fractal structures on Fe_3O_4 ferrofluid: a small-angle neutron scattering study. J. Phys. Conf. Ser. **247** (2010)
37. Tang, S.C.N., Lo, I.M.C.: Magnetic nanoparticles: essential factors for sustainable environmental applications. Water Res **47**, 2613–2632 (2013)

38. Petosa, A.R., Jaisi, D.P., Quevedo, I.R., Elimelech, M., Tufenkji, N.: Aggregation and deposition of engineered nanomaterials in aquatic environments: role of physicochemical interactions. Environ. Sci. Technol. **44**, 6532–6549 (2010)
39. Giri, J., Pradhan, P., Somani, V., Chelawat, H., Chhatre, S., Banerjee, R., Bahadur, D.: Synthesis and characterizations of water-based ferrofluids of substituted ferrites [$Fe_{1-x}B_xFe_2O_4$, B = Mn, Co (x = 0–1)] for biomedical applications. J. Magn. Magn. Mater. **320**, 724–730 (2008)
40. Rameshbabu, R., Ramesh, R., Kanagesan, S., Karthigeyan, A., Ponnusamy, S.: Synthesis and study of structural, morphological and magnetic properties of $ZnFe_2O_4$ nanoparticles. J. Supercond. Nov. Magn. **27**, 1499–1502 (2014)
41. Akbarzadeh, A., Samiei, M., Davaran, S.: Magnetic nanoparticles: preparation, physical properties, and applications in biomedicine. Nanoscale Res. Lett. **7**, 144 (2012)
42. Liu, X.-D., Chen, H., Liu, S.-S., Ye, L.-Q., Li, Y.-P.: Hydrothermal synthesis of superparamagnetic Fe_3O_4 nanoparticles with ionic liquids as stabilizer. Mater. Res. Bull. **62**, 217–221 (2015)
43. Caruntu, D., Caruntu, G., O'Connor, C.J.: Magnetic properties of variable-sized Fe_3O_4 nanoparticles synthesized from non-aqueous homogeneous solutions of polyols. J. Phys. Appl. Phys. **40**, 5801 (2007)
44. Tackett, R., Sudakar, C., Naik, R., Lawes, G., Rablau, C., Vaishnava, P.P.: Magnetic and optical response of tuning the magnetocrystalline anisotropy in Fe_3O_4 nanoparticle ferrofluids by Co doping. J. Magn. Magn. Mater. **320**, 2755–2759 (2008)
45. Şimşek, T., Akansel, S., Özcan, Ş.: Effect of hexane on magnetic blocking behavior of FePt nanoparticles. J. Magn. Magn. Mater **324**, 3924–3928 (2012)
46. Rumpf, K., Granitzer, P., Morales, P., Poelt, P., Reissner, M.: Variable blocking temperature of a porous silicon/Fe_3O_4 composite due to different interactions of the magnetic nanoparticles. Nanoscale Res. Lett. **7**, 445 (2012)
47. Thakur, S., Rai, R., Sharma, S.: Structural characterization and magnetic study of $NiFe_xO_4$ synthesized by co-precipitation method. Mater. Lett. **139**, 368–372 (2015)
48. Linh, P.H., Manh, D.H., Phong, P.T., Hong, L.V., Phuc, N.X.: Magnetic properties of Fe_3O_4 nanoparticles synthesized by coprecipitation method. J. Supercond. Nov. Magn. **27**, 2111–2115 (2014)
49. Gamarra, L.F., Pontuschka, W.M., Mamani, J.B., Cornejo, D.R., Oliveira, T.R., Vieira, E.D., Costa-Filho, A.J.J.r., Amaro, E.: Magnetic characterization by SQUID and FMR of a biocompatible ferrofluid based on Fe_3O_4. J. Phys. Condens. Matter. **21**, 115104 (2009)
50. Carta, D., Casula, M.F., Falqui, A., Loche, D., Mountjoy, G., Sangregorio, C., Corrias, A.: A Structural and magnetic investigation of the inversion degree in ferrite nanocrystals MFe_2O_4 (M = Mn, Co, Ni). J. Phys. Chem. C **113**, 8606–8615 (2009)
51. López, J., González-Bahamón, L.F., Prado, J., Caicedo, J.C., Zambrano, G., Gómez, M.E., Esteve, J., Prieto, P.: Study of magnetic and structural properties of ferrofluids based on cobalt–zinc ferrite nanoparticles. J. Magn. Magn. Mater. **324**, 394–402 (2012)
52. Dutta, P., Pal, S., Seehra, M.S., Shah, N., Huffman, G.P.: Size dependence of magnetic parameters and surface disorder in magnetite nanoparticles. J. Appl. Phys. **105**, 07B501 (2009)
53. Li, M., Gu, H., Zhang, C.: Highly sensitive magnetite nano clusters for MR cell imaging. Nanoscale Res. Lett. **7**, 204 (2012)
54. Goya, G.F., Berquó, T.S., Fonseca, F.C., Morales, M.P.: Static and dynamic magnetic properties of spherical magnetite nanoparticles. J. Appl. Phys. **94**, 3520–3528 (2003)
55. Zélis, P.M., Pasquevich, G.A., Stewart, S.J., van Raap, M.B.F., Aphesteguy, J., Bruvera, I.J., Laborde, C., Pianciola, B., Jacobo, S., Sánchez, F.H.: Structural and magnetic study of zinc-doped magnetite nanoparticles and ferrofluids for hyperthermia applications. J. Phys. Appl. Phys. **46** (2013)